GeoVirtual 2020 September 14-16
Resilience and Innovation

Seismic and post-seismic stability of tailings impoundments, considering the effect of reinforcement inclusions

Carlos Contreras, Samuel Yniesta, & Michel Aubertin
Department of Civil, Geological and Mining Engineering, Polytechnique Montréal, Montréal, Québec, Canada

ABSTRACT
Post seismic impoundment failures can be caused by the redistribution of excess interstitial pore water pressures generated during the seismic event or by the driving stresses that may exceed the available shear strength. This paper presents numerical analyses to evaluate the seismic and post seismic stability of a tailing impoundment, with and without waste rock inclusions. The tailings are modelled in the shaking phase using the PM4Sand constitutive model. The results show that the unreinforced impoundments (without inclusion) are subjected to medium to high displacements at the end of the shaking, and present two types of behaviour in the post-seismic phase: i) cases with controlled deformations for stable impoundment and ii) cases with increasing displacements leading to impoundment instability. Impoundments reinforced by waste rock inclusions show limited displacements under post seismic condition even when high pore water pressures developed during shaking.

RÉSUMÉ
Les ruptures post-sismiques des parcs à résidus peuvent être causées par la redistribution de la pression interstitielle en excès générée pendant l'événement sismique ou par des forces motrices qui dépassent la résistance au cisaillement disponible du sol. L'article présente des analyses numériques pour évaluer la stabilité sismique et post-sismique d'un parc à résidus, avec et sans inclusions de roche stériles. Les résidus sont modélisés dans la phase sismique à l'aide du modèle constitutif PM4Sand. Les résultats montrent que les parcs à résidus sans inclusions présentent des déplacements moyens à élevés à la fin du séisme, et présentent deux types de comportements dans la phase post sismique : i) déformations demeurent constantes (parcs stables) et ii) déformations augmentent constamment (parcs instables). Les parcs à résidus renforcés avec des inclusions de roche stériles présentent des déplacements limités dans des conditions post-sismiques, même lorsque le rapport de la pression interstitielle est élevé pendant la phase sismique.

1 INTRODUCTION

Hard rock tailings can be susceptible to both static and dynamic liquefaction (Vick, 1990; Bussière, 2007), which can cause the rupture of the retaining dikes and the runoff of tailings. Such failures have generated significant damages over the years, with loss of lives and dire environmental consequences in some cases.

The rupture of tailings impoundment can take place during a seismic event, as was the case for example at Cerro Negro (1965 and 1985), Hokkaido (1968), and Tapo Canyon (1994), (Ishihara,1984; Ishihara et al., 1990; Harder and Stewart, 1996; Villavicencio et al., 2014). Post-seismic ruptures can also occur after the seismic event, due to a redistribution of the excess interstitial pore water pressures generated during seismic loading or to the driving forces that may then exceed the available shear strength of the material. Examples of such delayed ruptures include the Lower San Fernando Dam (1971) (Seed et al., 1988) and the No 2 dike at the tailings impoundment in Mochikoshi (1978), which occurred about thirty seconds and one day respectively, after the earthquakes.

The evaluation of seismic and post seismic stability of tailings impoundments can be conducted using numerical modelling with recently developed constitutive models, such as UBCSAND (Beaty and Byrne, 2011) and PM4Sand (Boulanger and Ziotopoulou, 2017). Such simulations can lead to reliable results, as shown for instance by the back analysis of the Mochikoshi dike failure (Byrne and Seid-Karbasi, 2003). These fully coupled effective stress models can simulate the displacements and liquefaction (reduction of strength and stiffness) during an earthquake, with the pore water redistribution and dissipation during and after the event. Another option to analyze the post seismic stability of tailings impoundments is to apply a total stress approach with the residual (liquefied) strength for elements that were submitted to high pore water pressure ratios, r_u, at the end of the earthquake. This method gives similar results to fully

coupled models, but is less computing time-demanding (Naesgaard and Byrne, 2007; Naesgaard, 2011).

This paper presents the seismic and post-seismic analysis of hard rock tailings impoundments using numerical simulations. The tailings are modelled in the shaking phase using the PM4Sand (Boulanger and Ziotopoulou, 2017) constitutive model, with parameters calibrated on extensive laboratory and field-testing results (Contreras, 2021). In the post seismic phase, a total stress approach is used to analyze the stability of the impoundment with tailings having a shear strength reduced by the excess pore water pressures, using values consistent with laboratory test results (James et al., 2011; Golder, 2014; Archambault-Alwin, 2017). The use of waste rock inclusions (WRI) to improve the seismic and post-seismic stability is also considered in the simulations, as discussed below.

2 WASTE ROCK INCLUSIONS IN TALINGS IMPOUNDMENTS

Tailings and waste rock are two by-products of hard rock mining operations. Both types of waste can be managed more efficiently by placing waste rock as inclusions in the tailings impoundment to accelerate drainage and consolidation and increase static and seismic stability (Aubertin et al., 2002). The WRI technique consists in constructing a network of rows of waste rock inside the impoundment, with the inclusions and dikes raised sequentially as the tailings are deposited hydraulically.

The advantages of using this co-disposal method include a reduction of the storage volume for the waste rock (usually placed in piles), compartmentalization of the impoundment, a more rapid tailings consolidation with strength gain, and increased static and seismic stability (James et al., 2013). The WRI can be designed to improve slope stability for both static and seismic loading by increasing the resistance of tailings and adding reinforcement in the impoundment (Jahanbakhshzadeh et al. 2019; Jahanbakhshzadeh and Aubertin, 2020). The optimal design of the inclusions (width and spacing) depends on various factors, including the material properties and aimed improvements.

Previous studies by James et al. (2010), James and Aubertin (2012), Ferdosi et al. (2015a, 2015b), and Aubertin et al. (2019) have shown the effectiveness of WRI to improve the seismic stability, without providing design criteria. Other studies have focused on the improvement of consolidation with the inclusions (e.g. Jaouhar et al., 2013; L. Bolduc et Aubertin, 2014; Saleh Mbemba, 2016) and have demonstrated that the rate of excess pore water pressure dissipation is increased in the presence of inclusions, to a distance of about twice the tailings thickness.

In the following, the presence of WRI is analyzed to assess their effect on the post-shaking stability of tailings impoundments.

3 METHODOLOGY

3.1 Impoundment Configurations

The tailings impoundments considered in this numerical study include a starter dike and upstream raised dikes composed of waste rock, with a tailings thickness of 30 m (Figure 1a). Models with upstream slopes of 13H:1V and 9H:1V are analyzed. The foundation beneath the tailings is composed of a till layer overlying the bedrock. This configuration is fairly typical of what can be found in the Abitibi region, Québec. Some of models comprise waste rock inclusions to assess their reinforcement effect (Figure 1**Error! Reference source not found.**b)

3.2. Numerical Analysis Procedure

The numerical analyses were performed using the software FLAC 8.0 (Itasca, 2016). Each analysis is performed in 3 different stages: i) hydraulic and static equilibrium, ii) dynamic analysis, and iii) a post seismic phase.

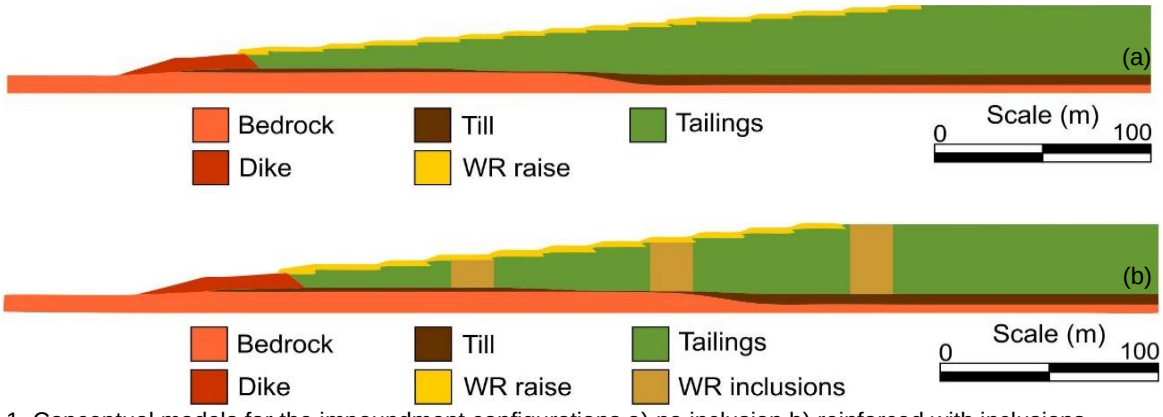

Figure 1. Conceptual models for the impoundment configurations a) no inclusion b) reinforced with inclusions

The static phase sets the state of stresses and pore water pressures at equilibrium before the earthquake loading is applied. In this initial phase, the elasto-plastic Mohr Coulomb constitutive model is used except for the bedrock which is considered linearly elastic. In the dynamic phase, the hard rock tailings are represented by the PM4Sand model to simulate their susceptibility to liquefaction, while the other materials retain the same (initial) constitutive model. A specific undrained shear strength is attributed to the tailings in the post-seismic phase (when liquefaction occurred).

3.3 Properties of the Materials

3.3.1 Static Phase

The results from previous studies were used to define the required properties of the tailings and waste rock (e.g. James, 2009; Ferdosi et al., 2015a). All the properties are presented in Table 1. A relatively small effective cohesion was assigned to the waste rock in dikes to avoid premature distortion of elements.

The bulk K and shear G moduli of the waste rock were considered as being a function of the effective stress. The relationship given by Seed and Idriss (1970) and adapted by James (2009) was used with minimum values of $3 \cdot 10^5$ kPa and $7 \cdot 10^5$ kPa respectively:

$$G = 55000 \cdot (0.6 \cdot \sigma_v')^{0.5} \quad [1]$$

$$K = 2.17 \cdot G \quad [2]$$

It is considered that the hard rock mine tailings are transported from the mill and deposited as a slurry in the impoundment. The geotechnical properties of hard rock tailings have been the subject of several studies (Vick, 1990; Qiu and Sego, 2001; Aubertin et al., 2002, 2011; Bussière, 2007; Blight, 2010). The typical characterization results used here indicate that the particle size distribution of tailings include 10% to 30% of sand, with the rest made of fine-grained particles (<75 μm). The average relative density D_r (or specific gravity G_s) of the particles varies from 2.6 to a 4.0. Atterberg limits tests indicate that the Plasticity Index is less than 10%. Hard rock tailings are commonly classified as non-plastic silt (ML) based on the Unified Soil Classification System (ASTM Standard D2487)

The behaviour of tailings strongly depends on their density (or porosity). In the impoundment, tailings consolidate under their own weight, and the Density Index, I_d, becomes a function of the effective vertical stress, σ'_v. In the simulations, the value of I_d, was set using Eq. 3 based on the experimental results of Essayad (2015) (see also Contreras, 2021), with a minimum value of 40%.

$$I_d = 0.326 \cdot \sigma_v'^{0.1} \quad (\geq 40\%) \quad [3]$$

For the 30 m-high tailings impoundment considered here, this function yields a density index between 40% and 57%.

In situ shear wave velocity measurements can also be performed on tailings (Grimard et al. 2020). Typical experimental values were converted into the small strain shear modulus, $G_{max.}$ which was then used to obtain the average shear modulus G and the corresponding vertical profiles for the static phase, based on the approximated in-situ density. A Poisson coefficient ν of 0.3 was used to estimate the bulk modulus K. The in-situ shear modulus profiles were used to obtain the best fit for parameter G_o with the PM4Sand model.

Table 1. Material properties

Properties	Tailings	Starter dyke	Till	Waste rock dikes	Waste rock inclusions	Bedrock
Dry density, ρ_d (Mg/m3)	Var	2.2	1.9	2.0	2.0	2.6
Effective friction angle, ϕ' (°)	37[1]	45	36	45	45	-
Effective cohesion, c' (kPa)	0.0	30	0.0	15	0.0	-
Dilation angle (°)	0.0	5.0	0.0	10	10	-
Porosity, n	0.4	0.3	0.3	0.3	0.3	0.25
Density index, I_d	Var.	-	-	-	-	-
Shear modulus, G (kPa)	Var.	5.6e5	3.6e5	4.1e5	Var.	23e6
Hydraulic conductivity (m/s)	2e-7	1e-3	5e-7	1e-3	1e-3	1e-9

[1]Static phase only

3.3.2 Dynamic Properties

The model Sig3 (Itasca, 2016) was used to simulate the shear modulus degradation and damping behaviour for all the materials other than the tailings and bedrock. The default values for granular materials were used for the till foundation and the calibrated values proposed by Ferdosi et al., (2015) were used for the waste rock. A stiffness and mass-dependent Rayleigh damping ratio of 0.5%, centered on the predominant frequency of the motion, was assigned to all materials to introduce small strain damping (Itasca, 2016; Boulanger and Ziotopoulou, 2017).

As indicated above, the tailings were modelled using the PM4Sand constitutive model (Boulanger and Ziotopoulou, 2017), with parameters calibrated on results obtained from extensive laboratory and field-testing programs (James, 2009; Poncelet, 2012; Golder, 2014; Essayad, 2015; Archambault-Alwin, 2017; Grimard, 2017 ; Boudrias, 2018). Table 2 presents the values used for the simulations; more details can be found in Contreras (2021).

Table 2. PM4Sand model calibrated parameters used in the simulations

Parameters	Hard rock tailings calibration
I_d- Apparent density index	Variable
G_o-Shear modulus coefficient	502.5
h_{po}-Contraction rate parameter	0.55
e_{min}-Minimum void ratio	0.49
e_{max}-Maximum void ratio	1.1

n_b- Bounding parameter	0.7
c_z- Fabric growth parameter	150
ϕ'_{cv}-Critical state friction angle	35
C_{GD}-Modulus degradation factor	2.5
Q- Critical state line parameter	12.7
R- Critical state line parameter	5.4

3.4 Input Ground Motions

The seismic hazard considered here is of moderate intensity, typical of the metal mining regions in the province of Québec, Canada. The design spectra for return periods of 2,475 and 10,000 years, based on a probabilistic seismic hazard analysis, are presented in Figure 2 (see Contreras, 2021, for more details). The peak ground accelerations (PGA) are 0.083 and 0.133g for the two return periods. A seismic hazard deaggregation analysis was performed and showed that the earthquake magnitude mode (M_w) controlling these seismic hazards varies from 6.7 to 7.3 for a 2,475-year return period, and 7.25 to 7.75 for a 10,000-year return period.

Ground motions compatible with the design spectra were selected from databases of NGA-East (Goulet et al. 2014) and NGA-West2 (Ancheta et al. 2013) and synthetic motions for Eastern regions of Canada (Atkinson, 2009). Although recordings from the East databases are more relevant for the seismic hazard in the considered region, there are only a few ground motions with the required intensities recorded that are compatible with the regional seismicity. Motions from the NGA-West2 were therefore considered also to provide a wider range of seismic loading conditions. The seismic hazards in the geographical region of interest is associated with high frequency ground motions, but alternative scenarios with low frequency motions were also considered for the purpose of studying this effect. The ground motions characteristics used in the simulations presented here are given in Table 3.

Table 3. East and West ground motions parameters

Name of event	M_w	PGA (m/s^2)	AI (m/s)	F_{pred} (Hz)
High-frequency content ground motions				
Saguenay	5.9	1.60	0.125	8.33
Sparks	5.7	0.66	0.125	8.33
Nahanni	6.8	1.69	0.127	16.67
Atkinson 7.0	7.0	1.16	0.127	16.67
Iwate	6.9	0.86	0.126	12.50
SOR	6.7	1.05	0.126	25.00
Chichi	7.6	1.45	0.125	10.00
Low-frequency content ground motions				
Loma Prieta	6.9	0.87	0.125	4.17
El Mayor	7.2	0.76	0.125	5.56
San Fernando	6.6	0.99	0.125	3.85
Morgan	6.2	1.40	0.125	7.14
Tabas	7.3	0.86	0.125	4.17
Kocaeli	7.5	0.89	0.125	3.57
Tottori	6.6	1.15	0.125	5.00

The seismic hazard is typically characterized using ground motion parameters such as spectral peak acceleration PGA and peak ground velocity PGV. Other ground motion intensity measures can also be used to evaluate the response of geotechnical systems such as tailings impoundments. For instance, liquefaction and its effects on site response can be assessed more precisely with cumulative intensity measures (such as the Arias Intensity AI or cumulative absolute velocity CAV) instead of using a single indicator value like the PGA or PGV (Kramer and Mitchell, 2006). The Arias intensity is chosen here to scale the selected ground motions.

The values of AI used in this study were computed from the relationships of Lee and Green (2010) and Farhadi and Pezeshk (2020), which are applicable for Central and Eastern regions of North America. Depending on the relationship and distribution of the mode in the deaggregation analysis, the AI values predicted by these equations varied between 0.032 to 0.122 m/s (for a 2,475-year return period) and 0.045 to 0.147 m/s (for 10,000 years). A single value of AI of 0.125 m/s was selected to scale all the ground motions in the simulations presented here; this value produces average spectra that match well the design spectrum in the range of periods of interest (0.3 to 1.0 s) for a return period of 10,000 years (as illustrated in Figure 2; see Contreras (2021) for more details).

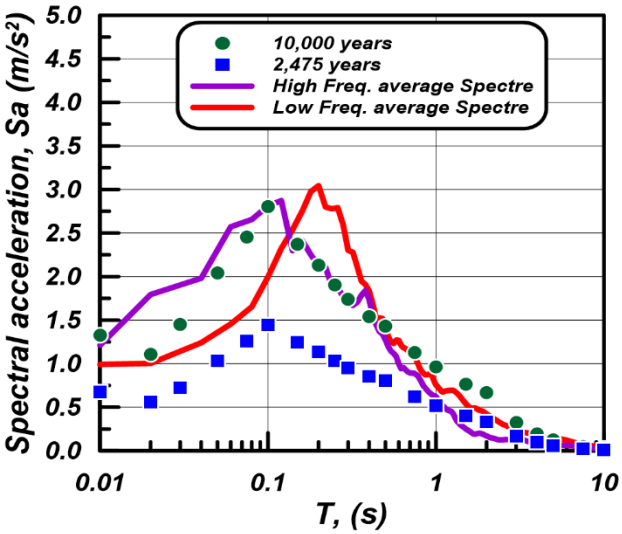

Figure 2. Design spectra considered in the simulations

3.5 Evaluation of Post-Seismic Stability

The values of shear and bulk moduli evaluated with the PM4sand model, modified from the initial values as a result of cyclic loading and pore pressure generation, are stored at the end of the dynamic analyses. These values are then used in conjunction with the elastoplastic Mohr Coulomb model to evaluate the post-seismic displacements and assess the impoundment stability. Laboratory tests have shown that post-cyclic strength can be expressed in term of the undrained shear strength ratio, s_u/σ'_v, for hard rock tailings, with a typical value of about 0.1 (James et al, 2011; Golder, 2014). This value of the residual (undrained) shear strength ratio (normalized by the pre-earthquake vertical effective stresses), with a minimal shear strength, S_u, of 10kPa, was assigned to the hard rock tailings elements where the pore water pressure ratio, r_u, equalled or

exceeded 0.7 at the end of shaking. At this value of r_u the cyclic shear strains become more pronounced, and it is commonly associated with a reduction of strength and stiffness due to the onset of liquefaction. An undrained shear strength ratio of 0.22 was assigned to the non-liquefied tailings elements. There was no change of properties for other materials. Each simulation is then conducted until the displacements stop or until one of the elements shows an excessive distortion.

4 MAIN RESULTS

4.1 Impoundments Without Inclusion

Dynamic analyses were performed for each impoundment model, with different slopes, using the motions presented in Table 3. Results such the ones in Figure 3 (for Nahanni) indicate that for the 13H:1V slope, the high-frequency ground motions lead to moderate displacements, ranging between 1.3 to 2.75 m, except for the recording from Sparks, which caused a larger displacement of 6.5 m at the end of the seismic phase. It is also observed that high r_u, values developed under the slope of the impoundment, indicating liquefaction of the tailings (Figure 3b). In most simulated cases, the liquefied zone is relatively shallow; the proportion of tailings liquefied varies between 10 and 35% of the total volume of tailings.

Low frequency ground motions (more typical of western regions) having identical Arias Intensity but on average lower PGA, caused the failure of the impoundment with a slope of 13H:1V in most cases (as illustrated in Figure 4 for the Kocaeli earthquake). For these motions, maximum displacements ranging from 6.5 to 9 m were obtained, except for the San Fernando motion, where a maximum of 2.75 m of displacement was computed at the end of the seismic phase. In general, the zone with high, r_u values developed deeper under the external slope of the impoundment, and this affected a larger volume, with a proportion of liquefied tailings varying from 23 to 57% of the total volume (e.g. Figure4b).

Post-seismic stability analyses showed that for high-frequency motions, three of the seven cases analyzed were unstable (including Sparks which was unstable during the seismic motion), as indicated by the continuously rising displacements in this phase. Examples of post-seismic behaviour for an unstable impoundment are shown in Figure *5* and 6. In Figure 5 (Nahanni earthquake), a displacement of 2.2 m due to the tailings liquefaction (r_u >0.8) under the slope is observed at the end of the earthquake. After 20 seconds in the post-seismic phase, the horizontal displacements increased to 3.5 m along the seismically induced failure surface. The figure also shows that horizontal displacements and velocities start to increase after about 4 seconds of seismic motion. Displacements continue to increase almost linearly over time, while velocities increased rapidly for about 7 seconds and then continued increasing at a lower rate. Once the post seismic phase starts (at 11 seconds), velocities decrease and remain essentially constant until the end leading to increasing displacements up to failure. The displacement and velocity time histories during and after the (simulated) low frequency Kocaeli earthquake are presented in Figure 6. The larger volume of liquefied tailings and the higher velocities generate much larger displacements (6.2m) in the seismic phase. Once the post seismic phase starts (at 22 seconds), velocities decrease and remain essentially constant until the end, leading to increasing displacements (1.0 m in 5 seconds) up to failure (7.5 m).

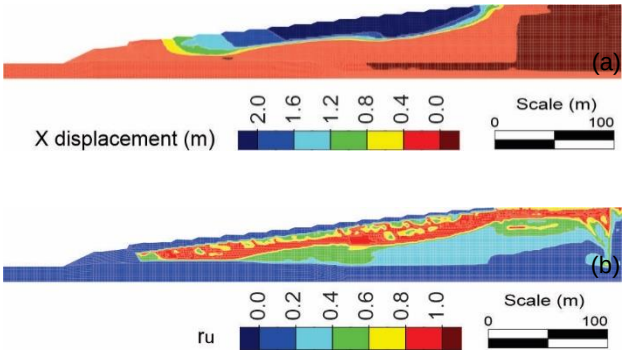

Figure 3. Results from the simulation of the impoundment without inclusion for a 13H:1 V slope a) Horizontal displacements (along the X axis) and b) Maximum pore water pressure ratio r_u, contours at the end of the high-frequency Nahanni earthquake

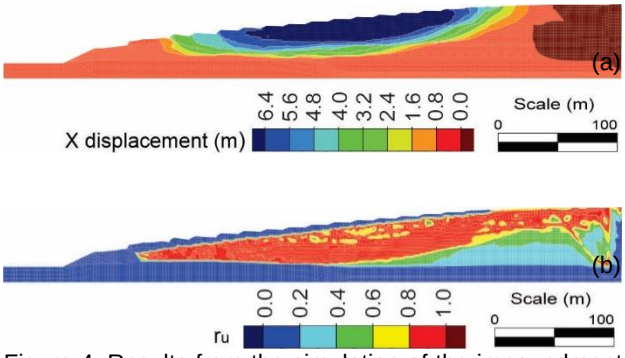

Figure 4. Results from the simulation of the impoundment without inclusion for a 13H:1V slope a) Horizontal displacements (along the X axis) and b) Maximum pore water pressure ratio r_u, contours at the end of the low-frequency Kocaeli earthquake

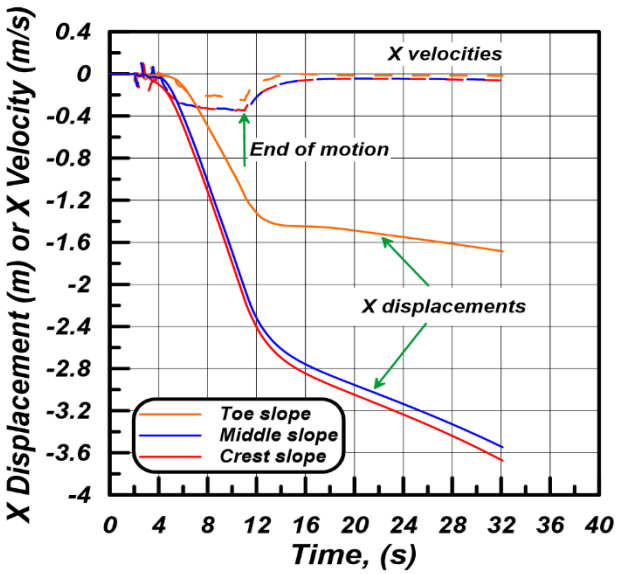

Figure 5. Seismic and post-seismic displacements and velocities along the 13H-1V slope, which lead to an unstable impoundment for the high frequency (Nahanni) seismic loading.

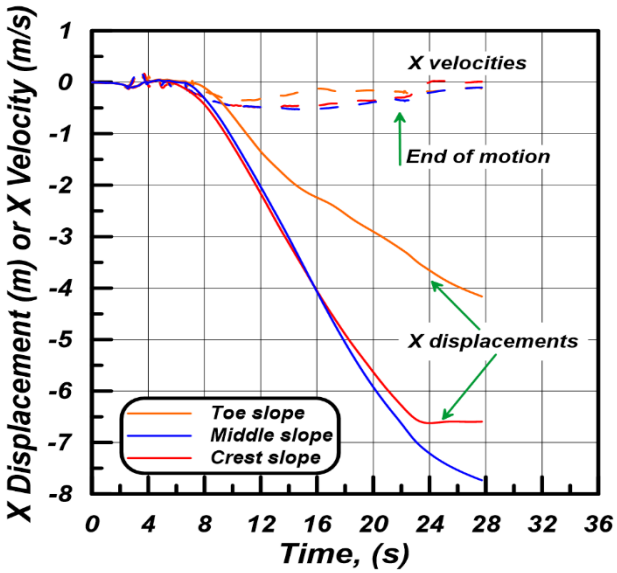

Figure 6. Seismic and post-seismic displacements and velocities along the 13H:1V slope, which leads to an unstable impoundment for the low frequency (Kocaeli) seismic loading.

Figure 7 and Figure 8 present the simulation results obtained for an impoundment subjected to the Saguenay earthquake, which would remain stable. At the end of the motion, the maximum displacement of 1.5 m seems to be insufficient to induce failure, although part of the tailings have liquefied and created an apparent slip surface. In comparison to the previous cases (Fig. 5 and 6), the extent of the liquefaction zone is smaller. The post-seismic results show that the horizontal displacements reached 1.5 to 1.7 m in 3 seconds and then remained stable (Figure 8). In the seismic phase, horizontal displacements and velocities increased from 9.5 seconds onward, with the displacements increasing rapidly and almost linearly over time, while velocities increased until reaching a plateau after about 12 seconds. Once the post seismic phase starts at 16.5 seconds, velocities decrease rapidly and become almost nil, indicating that the impoundment would likely remain stable.

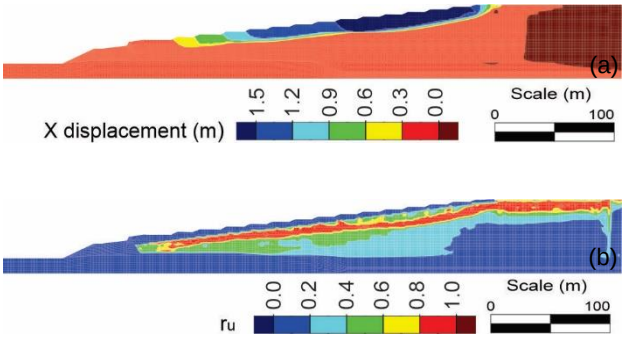

Figure 7. Results from the simulation of the impoundment without inclusion for a 13H:1V slope a) Horizontal displacements (along the X axis) and b) Maximum pore water pressure ratio r_u, contours at the end of the high-frequency Saguenay S49 earthquake

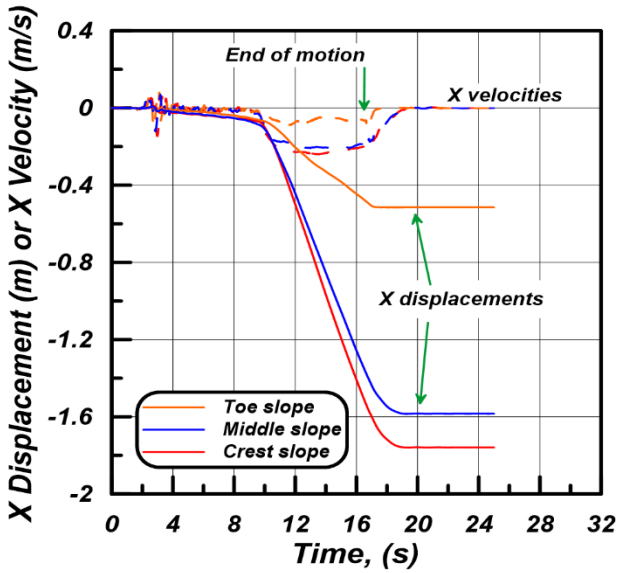

Figure 8. Seismic and post-seismic displacements and velocities along the 13H:1V slope, which leads to an apparently stable impoundment for the high frequency (Saguenay) seismic loading.

The post seismic analyses of the impoundment models with a 13H:1V slope indicated that three of seven analyses for high-frequency motions and five of seven cases with low-frequency motions were showing continually rising displacements, indicative of unstable slopes.

The analyses for the impoundment models with a slope of 9H:1V led to higher velocities and displacements rates

and produced fewer stable cases. The number of unstable simulations for high-frequency motions increase to five out of seven; for low-frequency motions, all motions induce failure.The proportion of volume liquefied for low-frequency motions is typically much larger than for high-frequency motions, as was also observed for the 13H:1V slope models.

Post seismic analyses producing small deformations tend to indicate that failure should not occur (because the residual strength is not exceeded). When deformations become larger, there is a stronger potential for liquefaction and flow failure (Naesgaard, 2011). However, the threshold deformation at which the liquefaction induced failure would occur is not well defined.

Based on the available indications, most of cases analyzed in this study could lead to a flow failure of the tailings impoundment model. However, as seen in some cases, it appears that relatively large movement of liquefied mass tailings can sometimes stop so the impoundment could remain stable. More work is underway to further analyze this type of behavior.

4.2 Effect of Waste Rock Inclusions

Results in the previous section indicates that the unreinforced impoundments are susceptible to become unstable under dynamic loading, either during the earthquake or shortly after. In this section, simulation results are presented to assess the stability of impoundments reinforced with waste rock inclusions.

Designing WRI involves selecting the spacing between the inclusions and their width. For consolidation purposes, previous analyses have shown that the effective distance can extent up to twice the tailings thickness on each side, with the main efficiency occurring over a distance equals to about the tailings height in the impoundment (L. Bolduc and Aubertin, 2014; Saleh Mbemba and Aubertin, 2019). Therefore, the spacing between the inclusion for the 30 m thick impoundment was fixed at 60 m here. The width of the WRI is set to 15 m, based on field experience. The effect of the inclusions is presented here using simulation results with the earthquake Tabas (see Table 3), which produced one the largest displacements and volume of liquefied tailings for the two slope angles analyzed (without and with inclusions).

The waste rock inclusion configuration in the impoundment is presented in Figure 9 for the 9H:1V slope (the configuration of the model with the 13H:1V slope was similar). The first inclusion is located at 60 m from the starter dike, and the others are placed with the same spacing up to (near) the crest of the slope.

The results of the simulations shown in Figure 9, for cases without and with inclusions, indicate that the WRI can reduce the volume of liquefied tailings (by up to 40%) in the impoundment, as well as the displacements (up to a factor or 5) The same tendencies are obtained for the steeper (9H:1V) and gentler (13H:1V) slopes (not shown here; see Contreras (2021) for details). The reduction of the volume of liquefied tailings and of the related displacements is mainly due to the global increase of stiffness of the impoundment provided by the WRI. The reduction of liquefied tailings volume obtained here differs from the results obtained by James (2009) and Ferdosi et al. (2015b), who reported that the inclusions didn't affect much the tailings liquefaction in the impoundment. This difference can be related, at least in part, to the higher levels of energy of the earthquake used in these earlier studies (AI 2.0 à 3.0 m/s), and to the different constitutive models used; this aspect is addressed in more details by Contreras (2021).

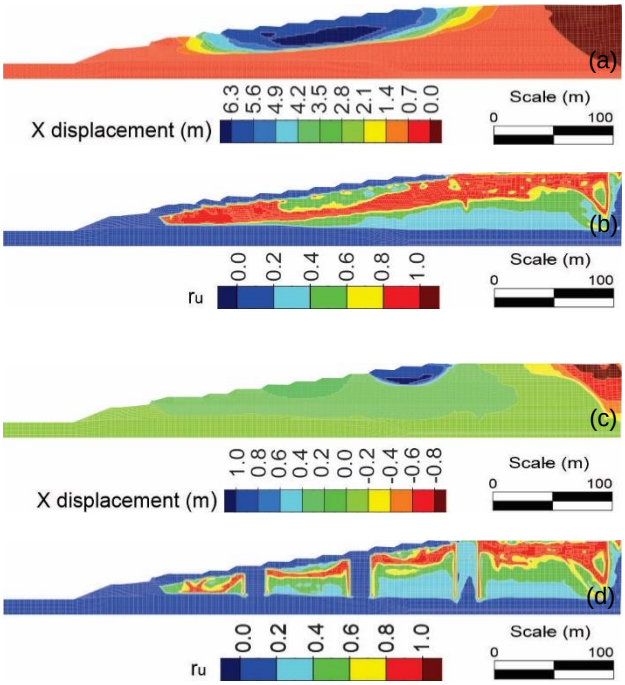

Figure 9. Results from the simulation of the impoundment with and without inclusion for a 9H:1V slope at the end of shaking a) Horizontal displacements (along the X axis) without inclusion and corresponding b) Maximal, r_u, ; c) Horizontal displacements (along the X axis) with inclusion and corresponding d) Maximal, r_u, with inclusions (low frequency Tabas earthquake).

The results indicate that the WRI reduce the maximal velocities during the seismic phase, resulting in an increased stability compared to the impoundment without inclusions (Figure 10 and 11). The results for the post seismic phase (Figure 11) indicate that the increased stiffness of the system also limits the displacement of the liquefied tailings. These results, and other similar ones, show that the waste rock inclusions (initially designed to improve consolidation) can increase the stability of impoundments; in many cases, this reinforcement would be sufficient to withstand the seismic hazard without a breach (which could be otherwise induced).

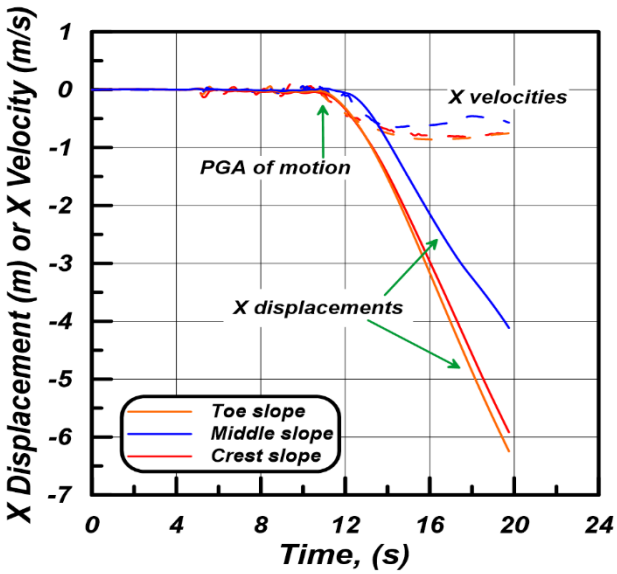

Figure 10. Seismic displacements and velocities for the unreinforced (without inclusion) impoundment along the 9H:1V slope, which leads to an unstable impoundment for the low frequency (Tabas) seismic loading.

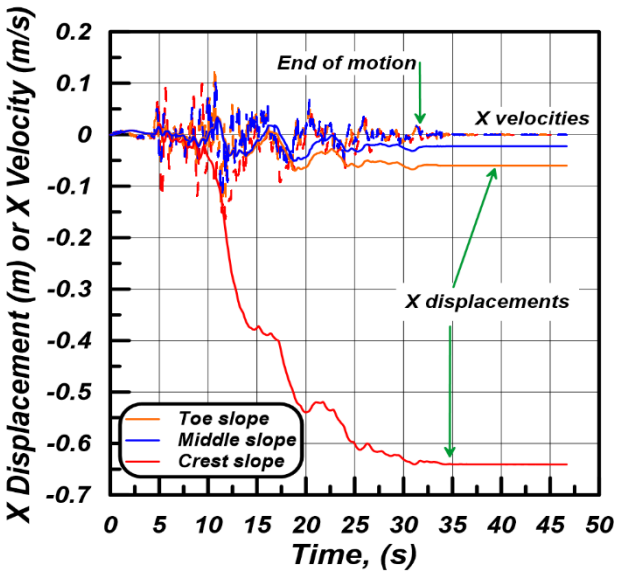

Figure 11. Seismic displacements and velocities for the reinforced (with inclusions) impoundment along the 9H:1V slope, which leads to a stable impoundment for the low frequency (Tabas) seismic loading

5 CONCLUSION

This paper presents results of analyses of the seismic and post-seismic stability of tailings impoundments with dikes built upstream. The simulations results indicate that unreinforced impoundments with a 9H:1V slope are likely to fail, under low and high frequency content motions. Impoundments with a gentler slope of 13H:1V are less likely to fail. Increasing the slope of the dikes causes higher velocities along the slope of the impoundments, which imply a higher rate of displacements more likely to lead to failure.

Earthquake motions with a lower frequency content typically produce more critical conditions that are more likely to induce failure, even for identical levels of Arias Intensity. Also, high-frequency motions induce a lower volume of liquefied tailings, compared with low-frequency motions.

The use of waste rock inclusions is shown to improve the seismic and post-seismic stability and thus reduce the risk of failure. Results also indicate that for the conditions considered here, the increased stiffness of the impoundment due to inclusions can reduce the volume of liquefied tailings and displacement, velocities, and thus contributes to seismic stability. The inclusions also compartmentalize the impoundment and reduce the amount of soil mass involved in the displacements, even when tailings are liquefied, because of the confinement between the inclusions.

6 ACKNOWLEDGEMENTS

This research work is being supported by the Research Institute on Mines and the Environment (RIME UQAT-Polytechnique; www.rime-irme.ca) and its partners.

7 REFERENCES

Ancheta, T. D., et al. 2013. PEER NGA-West2 database. Berkeley, CA: Pacific Earthquake Engineering Research Center.

Archambault-Awin, X. 2017. Évaluation du comportement dynamique et de la résistance cyclique des résidus miniers. M.Sc.A. thesis, Département des génies civil, géologique et des mines, École Polytechnique de Montréal. Montréal, Q.C.

ASTM Standard D2487-17.2017. Standard practice for classification of soils for engineering purposes.

Aubertin, M., Mbonimpa, M., Jolette, D., Bussiere, B., Chapuis, R.P., James, M., et Riffon, O. 2002. Stabilité géotechnique des ouvrages de retenue pour les résidus miniers: problèmes persistants et méthodes de contrôle. *Défis & Perspectives : Symposium sur l'environnement et les mines*, Développement Économique Canada/Ministère des Ressources Naturelles du Québec/CIM, Rouyn-Noranda, Québec, Canada.

Aubertin, M., Mbonimpa, M., Jolette, D., Bussière, B. Chapuis, R. James,M. and Riffon, O., et al. 2011. Stabilité géotechnique des ouvrages de retenue pour les résidus miniers: problèmes persistants et méthodes de contrôle. Online. http://www.envirogeremi.polymtl.ca/pdf/articles consulted 12 May 2016.

Aubertin, M., Jahanbakhshzadeh, A., Yniesta, S. 2019. The effect of waste rock inclusions on the seismic stability of a tailings impoundment. Proceedings of 7th International Conference on Earthquake Geotechnical Engineering.

Atkinson, G.M. 2009. Earthquake time histories compatible with the 2005 NBCC uniform hazard spectrum. Canadian Journal of Civil Engineering, 36 (6): 991-1000

Beaty M.H., and Byrne, P.M. 2011. UBCSAND constitutive model, Version 904aR. Document report: UBCSAND constitutive model on Itasca UDM web site.

Blight, G. 2010. Geotechnical engineering for mine waste storage facilities. Taylor & Francis Group, London. Google Scholar

Bolduc, F., and Aubertin, M. 2014. Numerical Investigation of the Influence of Waste Rock Inclusions on Tailings Consolidation. *Canadian Geotechnical Journal*, 51: 1021-1032.

Boudrias, G. 2018. Évaluation numérique et expérimentale du drainage et de la consolidation de résidus miniers à proximité d'une inclusion de roches stériles M.Sc.A. thesis, Département des génies civil, géologique et des mines, École Polytechnique de Montréal. Montréal, Q.C.

Boulanger, R.W., and Ziotopoulou, K. 2017. PM4Sand (version 3.1): A sand plasticity model for earthquake engineering applications. Center for geotechnical modelling. Report No UCD/CGM-17-01.

Bussière, B. 2007. Colloquium 2004: Hydrogeotechnical properties of hard rock tailings from metal mines and emerging geoenvironmental disposal approaches. *Canadian Geotechnical Journal*, 44(9): 1019-1052

Byrne, P. M., and Seid-Karbasi, M. 2003. Seismic stability of impoundments. *17th Annual Symposium, Vancouver Geotechnical Society*. Vancouver, Canada

Contreras, C.A. 2021. Détermination de la stabilité sismique et post-sismique des parcs à résidus de roche dure avec et sans inclusions de roche stérile pour des aléas faibles, intermédiaires et élevés des régions minières de l'est du Canada. Thèse de doctorat, Département civil, géologie et Mines, École Polytechnique de Montréal, Québec, Canada. En préparation

Essayad, K. 2015. Développement de protocoles expérimentaux pour caractériser la consolidation de résidus miniers saturés et non saturés à partir d'essais de compression en colonne. M.Sc.A. thesis, Département des génies civil, géologique et des mines, École Polytechnique de Montréal. Montreal, Q.C.

Farhadi, A. and Pezeshk, S. 2020. A referenced empirical ground-motion model for Arias intensity and cumulative absolute velocity based on the NGA-East database. *Bulletin of the seismological society of America*, 110: 508-518.

Ferdosi, B. James, M. Aubertin, M. 2015(b). Effect of Waste Rock Inclusions on the Seismic Stability of an Upstream Raised Tailings Impoundment: A Numerical Investigation. *Canadian Geotechnical Journal*, 52: 1930-1944.

Ferdosi, B. James, M. Aubertin, M. 2015(a). Investigation of the effect of waste rock inclusions configuration on the seismic performance of a tailings impoundment. *Geotechnical and Geological Engineering*, 6: 1519-1537.

Golder. 2014. Rapport de caractérisation des résidus miniers. 021-13-1221-0020-3020-RF-Rev0

Goulet, C. A., et al. 2014. PEER NGA-east database. Berkeley, CA: Pacific Earthquake Engineering Research Center

Grimard, L.P. 2017. Étude de laboratoire du comportement de résidus miniers soumis à des essais de compression non drainés et à une baisse du confinement, avec mesures de vitesse des ondes de cisaillement. M.Sc.A. thesis, Département des génies civil, géologique et des mines, École Polytechnique de Montréal. Montreal, Q.C.

Grimard, L.P., Karray, M., James, M., and Aubertin, M. 2020. Consolidation characteristics of hydraulically deposited tailings obtained from shear wave velocity (Vs) measurements in triaxial and oedometric cells with P-RAT. *Canadian Geotechnical* Journal. Manuscript submitted for publication

Harder, L.F. and Stewart, J.P. 1996. Failure of Tapo Canyon tailings dam. *Journal of performance of constructed facilities*, ASCE, 103(3): 109-114.

Ishihara, K. 1984. Post-earthquake failure of a tailings dam due to liquefaction on the pond deposit. *Proceedings international conference on case histories in geotechnics engineering*, St. Louis, Mo.

Ishihara, K., Yasuda, S. and Yoshida, Y. 1990. Liquefaction induced Flow failure of embankments and residual strength of silty sands. *Soil and foundation*, 30: 69-80.

Itasca Consulting Group, Inc. (Itasca). 2016. FLAC – Fast Lagrangian Analysis of Continua. Version 8.00. Computer software and user manual. Itasca Consulting Group, Inc., Minneapolis, Minn.

Jahanbakhshzadeh, A., Aubertin, M., Yniesta, S., Zafarani, A. 2019. On the seismic response of tailings dikes constructed with the upstream and center line methods. Geosciences for Sustainability. Proceedings of the 72th CGS Conference, St. John's, Canada.

Jahanbakhshzadeh, A. and Aubertin, M. 2020. The effect of waste rock inclusions on the slope stability of tailings dike. Proceedings of the 73th Canadian Geotechnical Society Conference, Calgary, Canada

James, M. 2009. The use of waste rock inclusions to control the effects of liquefaction in tailings impoundments. Thèse de Ph.D, Génie Minéral, École Polytechnique de Montréal, Québec, Canada.

James M, Aubertin A. 2010. On the dynamic response of tailings and the stability of tailings impoundments for hard rock mines. *Geotechnical News* 23(3): 39-43.

James, M., Aubertin, M., Wijewickreme, D., and Wilson, G. W. 2011. A laboratory investigation of the dynamic properties of tailings. *Canadian Geotechnical Journal*, 48(11): 1587-1600.

James, M., and Aubertin, M. 2012. The use of waste rock inclusions to improve the seismic stability of tailings impoundments. *GeoCongress American Society of Civil Engineers 2012*, Oakland, California: 4166–4175.

James, M., Aubertin., and Bussière, B. 2013. On the use of waste rock inclusion to improve the performance of tailings impoundments. *Proceedings of the 18th International conference on Soil mechanics and Geotechnical Engineering, Paris, France*.

Jaouhar, E.M. Aubertin, M. et James, M. 2013. The effect of tailings properties on their consolidation near waste

rock inclusions. *Proceedings of the 66th Canadian Geotechnical Conference*, Montréal, Québec, Canada.

Kramer, S.L. and Mitchell, R.A. 2006. Ground motion intensity measures for liquefaction hazard evaluation. *Earthquake spectra*, 22: 413-438.

Lee, J. and Green, R.A. 2010. And empirical Arias intensity relationship for rock sites in stable continental regions. *Proceedings of International conference on earthquakes engineering*, Tokyo, Japan.

Naesgaard, E., and Byrne, P.M. 2007. Flow liquefaction simulation using a combined effective stress – total stress model. *60th Canadian Geotechnical Conference*, *Canadian Geotechnical Society*,Ottawa, Ontario: 943–950.

Naesgaard, E. 2011. A hybrid effective stress – total stress procedure for analyzing soil embankments subjected to potential liquefaction and flow. Ph.D. thesis, Civil Engineering Department, University of British Columbia.

Poncelet, N. 2012. Élaboration et implémentation d'un protocole de laboratoire pour l'étude du potentiel de liquéfaction de résidus miniers. Mémoire de maitrise, Génie minéral, École Polytechnique de Montréal, Québec, Canada.

Qiu, Y. et Sego, D.C. 2001. Laboratory properties of mine tailings. *Journal Canadien de Geotechnique*, 38: 183–190.

Saleh Mbemba, F. 2016. Analyse et optimisation de la performance des inclusions rigides Durant la consolidation, le drainage et la dessiccation des résidus miniers. Ph.D. thesis, Département des génies civil, géologique et des mines, École Polytechnique de Montréal. Montréal, Q.C.

Saleh Mbemba, F. and Aubertin, M. 2019. Drainage and consolidation of mine tailings near waste rock inclusion. Paper presented at the 2019 ICOLD 87th Annual Meeting and Symposium, Ottawa, On, Canada.

Seed, H.B., and Idriss, I.M. 1970. Soil moduli and damping factors for dynamic response analyses. Earthquake Engineering Research Center, Berkeley, Calif. Report No. EERC 70-10.

Seed, H.B., Seed, R.B., Harder, L.F. and Jong, H.L. 1988. Re-evaluation of the Slide in the Lower San Fernando Dam in the Earthquake of Feb. 9, 197 1, Report No. UCB/EERC88/04, EERC and UC Berkeley.

Villavicencio, G., Espinace, R., Palma, J., Fourie, A. and Valenzuela, P. 2014. Failures of sand tailings dams in a highly seismic country. *Canadian Geotechnical Journal*, 51: 449-464.

Vick, S. G. 1990. Planning, design and analysis of tailings dams. Vancouver, BC: BiTech Publishers Ltd.